Science of the Total Environment 979 (2025) 179411

Contents lists available at ScienceDirect

Science of the Total Environment

journal homepage: www.elsevier.com/locate/scitotenv

Hydrological and geochemical controls of surface water and suspended sediment toxic metal fluxes from nearshore large coal ash pond

Stephen Anderson [a,*], Natasha T. Dimova [a], Dini Adyasari [b]

[a] Department of Geological Sciences, University of Alabama, Tuscaloosa, AL 35487, USA
[b] Department of Marine and Coastal Environmental Science, Texas A&M University at Galveston, TX, USA

HIGHLIGHTS

- High river flow controlled major metal concentrations in surface waters
- Environmental conditions impacted toxic metal concentrations across the transect
- Both As and Cd reached severe contamination in sediments during dry season
- Metals in sediment and water increased at shallow river channel depths in all seasons

GRAPHICAL ABSTRACT

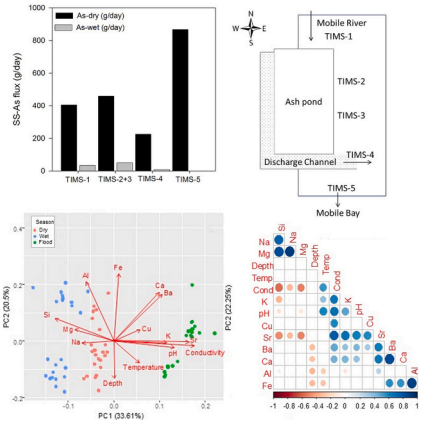

ARTICLE INFO

Editor: Bo Gao

Keywords:
Coal ash
Suspended sediments
Surface waters
Metal contamination
Seasonal variations

ABSTRACT

Toxic metals leached from ash coal ponds can pose a severe hazard to waterways and coastal areas. Observed toxic metal levels in surface waters near the largest ash pond in the Mobile-Tensaw Delta, Alabama, were the result of the interplay of multiple factors, including the specific chemical properties of individual metals and in situ environmental conditions driven by seasonal hydrological controls and flooding versus non-flooding conditions. We found that erosion and sediment resuspension after a significant rain event and flooding resulted in nearly double increase of major and trace metal concentrations in surface waters compared to non-flooding conditions. However, aluminium-iron (Al—Fe) co-precipitation and flocculation also controlled trace metal levels in surface water, especially during the dry season when seawater with higher pH and salinity from Mobile Bay propagated upstream. The highest arsenic (As) content in suspended sediments (44.6 mg/kg) was found near the Coal Power plant's discharge channel during the dry season. This level is similar to legacy contaminations found following the Kingston, TN ash spill (10 to 57 mg/kg). Higher river flow was associated with higher suspended sediment and suspended sediment-bound trace metal fluxes. However, when analyzing contaminated sediments near the ash pond, trace metal fluxes during the dry season exceeded the wet season, and ultimately, enrichment of As and Cd was observed near the discharge channel. These findings aim to promote research in

* Corresponding author.
E-mail address: swanderson1@crimson.ua.edu (S. Anderson).

https://doi.org/10.1016/j.scitotenv.2025.179411
Received 29 October 2024; Received in revised form 8 April 2025; Accepted 9 April 2025
0048-9697/Published by Elsevier B.V.

similar environments impacted by coal ash and to more comprehensively understand the relationship between toxic metals' partitioning and seasonal environmental conditions within the Mobile-Tensaw Delta.

1. Introduction

With an annual freshwater discharge of >1900 m^3/s, the Mobile Bay Estuary is the fourth largest estuary in the Continental US (Miller and Robinson, 1995). About 17 million cubic meters of coal ash is stored in an unlined pond by Plant Barry, an Alabama local power coal-combustion plant within the Mobile-Tensaw Delta, previously recognized as the "America's Amazon" by the naturalist E. O. Wilson. At this location, the coal ash pond is also <90 km from the Gulf of Mexico. The coal ash storage pond is primarily comprised of a mix of bottom and fly ash which enters the pond through sluiced flows as a slurry and is eventually captured by a discharge channel along with stormwater drainage when precipitation occurs. This ash pond also receives an influx of riverbank sediments that have been eroded during flooding. Ultimately, the combined sediment flux enters the adjacent Mobile River through subsequent surface runoff. For comparison, the Plant Barry ash pond near Mobile Bay, subject to storm surges, flooding, and sea level rise, is about four times the volume of US history's most disastrous ash spill at Kingston, TN, in 2008 (Ruhl et al., 2010; Dzwonkowski et al., 2015). Previous studies evaluating toxic metal contaminations in the Mobile River Basin, Alabama, indicate a positive correlation between river flood events and higher metal fluxes carried by sediments (Warner, 2005; Khaska et al., 2015). State, federal, and non-profit organization reports suggest that the most likely toxic metal pollution source to the downstream Mobile-Tensaw Delta and Mobile Bay is the historically well-established coal industry (Callaway et al., 2018). There are nine coal-fired power plants (CFPPs) along the Mobile River Basin, and 44 ash storage ponds associated with them, making Alabama the state with the largest amount of coal ash stored.

Coal ash storage ponds for convenience located near coal-fired power plants are enriched in toxic metals, including arsenic (As), barium (Ba), cadmium (Cd), cobalt (Co), cromium (Cr), copper (Cu), and lead (Pb), to mention a few (Mehra et al., 1998; Jegadeesan et al., 2008; Hussain et al., 2018). Since the ash contains naturally occurring radioactive elements such as uranium (U) and thorium (Th), the ponds could also be considered a radiation hazard during extreme weather events should the pond wall be breached. Hence, overall, there is a plausible concern for acute and chronic toxic metals environmental pollution from the Alabama ash pond, considering rising seawater levels and more frequent severe storm surges in the region since its initial construction (Mehra et al., 1998; Harkness et al., 2016; Roseburrough and Wang, 2019).

Metal contaminants travel through river systems via different mechanisms, including (i) as particle-bound elements to sediments in a solid state, (ii) as organic matter complexes and aggregates in the colloidal state (i.e., flocculates), and (iii) dissolved in the aqueous phase (Peng, 2008; Harkness et al., 2016). Suspended sediment (SS) particles have large effective surfaces, i.e., large surface area per unit mass, and, thus, high affinity to adsorb metals and pollutants, acting as effective long-distance transporting agents. Environmental conditions, such as surface water ionic strength, temperature, redox conditions, and pH, control the metals' state in the environment. At lower salinities (up to 2 ppt), flocculation, i.e., the colloidal aggregation of organic matter and fine sediment particles, dictates the transport mechanism of heavy metal contaminants within estuarine environments (Asgari et al., 2023). Under such conditions, heavy metals bind to flocs, which either settle into the estuarine sediments or are transported farther, altering their distribution and concentration profiles. On the other hand, when the fluvial SS plume encounters coastal waters with higher ionic strength, metals such as Cu, Pb, nickel (Ni), and zink (Zn) desorb from fine-grained sediments and enter the system in aqueous phase at varying rates (Miranda et al., 2022). Research investigating the desorption rates of metals in Australian estuarine environments concluded that Cd, Zn, and Co enter the dissolved state at much higher rates in saltwater, and the desorption is much less affected by pH (7.5–8) (Hatje et al., 2003). Another study reported that the variability of toxic metals (e.g., Cu) was higher during the summer and was attributed to the enhanced microbial activity at higher temperatures in summer (Braungardt et al., 2003).

Despite the urgency for comprehensive environmental assessments of the Plant Barry ash pond area, seasonal toxic metal evaluations have not been conducted outside of limited testing by the Southern Environmental Law Center in 2016. The primary goal of this research was to fill this knowledge gap by answering the following essential questions: (i) Are toxic trace metals, typically associated with coal ash, present at elevated levels in the Mobile River surface water (SW) and SS adjacent to Plant Barry's ash pond? And if so, what is the source? (ii) What environmental conditions control the toxic metals in dissolved state and suspended sediments in surface waters under different river flow regimes?

To answer the first question, we collected SS and SW across a 6-km section of the Mobile River near the Plant Bary ash pond over different seasons and calculated established contamination indexes. To determine the source contributions of SS as carriers of toxic metals, we divided the sampled river transect into four significant sections representative of the main sediment endmembers. We evaluated each contribution using a metal content-specific mass-balance mixing model approach. Finally, using statistical analyses (i.e., Principal Component Analysis (PCA) and Pearson correlations), we identified the governing hydrological and environmental parameters, including precipitation, stream flow, temperature, pH, conductivity, dissolved oxygen, and channel depth, that control the geochemical metal behavior and hence their spatial and temporal variability in suspended sediments and surface waters during dry, wet, and post-flooding river regimes.

We hypothesized that the mobile phase, i.e., dissolved coal ash-associated metals in surface waters near the pond, will be regulated mainly by short-term hydrological, marine and environmental controls, such as sudden rain events, episodic discharges from Plant Barry via the Sister's Creek discharge channel, tidal stages, etc. On the other hand, we expect suspended sediment fluxes and metals carried by them to change seasonally, i.e., higher river discharge to be associated with higher SS-bound metal fluxes as the primary way of metal transportation.

2. Study site

The study area near the Plant Barry ash pond is a 6-km section of Mobile River, which is the receiving point of the Mobile River Basin (MRB) (Fig. 1). The MRB covers about two-thirds of Alabama, spanning four physiographic provinces. Previous research has estimated a sedimentation rate of approximately five million tons per year from the Mobile River Basin through the associated Mobile-Tensaw Delta (M-T Delta), with the majority being deposited in the Mobile Bay (Davis, 2017).

The study site falls within the Eastern Gulf Coastal Plain province, with soils primarily comprised of peat, high organic matter sand, and fine-grained sediments (e.g., clays) deposited from the Upper MRB. Most of the land use land cover (LULC) of the Mobile-Tensaw Delta and the Plant Barry ash pond is forest (60 %), along with agriculture (26 %) and low-lying wetlands, streams, and reservoirs (11 %)(Warner et al., 2005).

Recent environmental reports have revealed high As, Cr, and Se concentrations in groundwater collected near the ash pond, with some of the toxic metals (e.g., Cr) up to 680 % of EPA max contaminant levels. As a result of the last few decades of gradual sea level rise following initial construction in 1954, the ash pond is currently located within the 100-

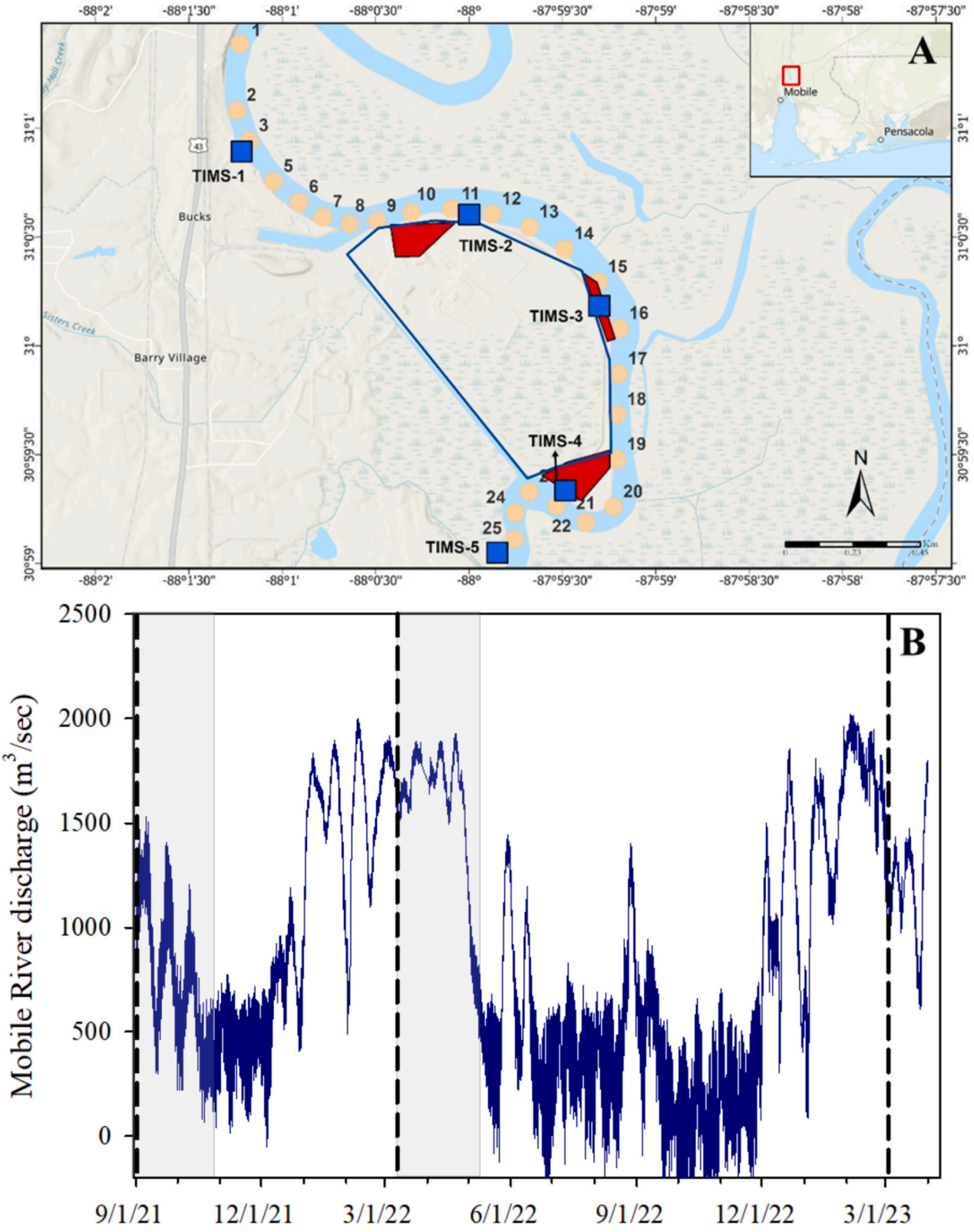

Fig. 1. The top panel (A) illustrates the study site and sampling locations near the Plant Barry ash pond. The perimeter of the ash pond is indicated by the thick blue outline. Light brown circles indicate surface water sample locations and blue squares represent suspended sediment sampler (TIMS) positions. Red areas highlight suspected contamination locations from previous reports evaluating surface runoff and groundwater wells at the sample site. The bottom panel (B) depicts the hydrological conditions at the closest stream gauge at the Mobile River (USGS 02470629). This stream gage is located directly to the west of the SW 1 sampling position. Highlighted grey areas represent the periods of TIMS deployments, while dashed lines represent the three surface water sampling campaigns.

year floodplain of the M-T Delta and its higher groundwater table includes isolated clay lenses allowing for toxic metal transport to the river system (Callaway et al., 2018). Fly ash transported through increased runoff to the M-T Delta during high precipitation events was evident during our field sampling events and has also been reported by other regional studies (Callaway et al., 2018; Vengosh et al., 2019; Wang et al., 2022).

Diurnal tidal variations of the downstream Mobile Bay Estuary control the spatial and temporal, hourly to daily, environmental conditions in the study area. On a longer time scale, i.e., seasonally, precipitation regulates the Mobile River discharge, which affects the adjacent surface water quality near the study site (Fig. 1A). The average monthly precipitation of the area is 53 mm. Generally, the dry season is June–September, but extending until the end of November is not uncommon, while the rainy season is in the early spring (March–June). Episodic large-scale storm events initiated in the Gulf of Mexico during the summer and late fall can quickly alter the study area's hydrodynamics and in-situ environmental conditions (Montiel et al., 2018; Adyasari et al., 2021). These extreme events have often historically occurred in the M-T Delta and Mobile Bay Estuary, causing large-scale flooding and structural damage to essential infrastructure. For example, a few of the most significant storms on the Alabama coast, i.e., Hurricane Fredrick (1976), Hurricane Ivan (2004), and Hurricane Sally (2020) have occured during the month of September (Azziz-Baumgartner et al., 2005; Totten et al., 2020). The combination of hydrological and marine controls on small and large scales and extreme conditions is expected to significantly impact the transport, distribution, and magnitude of toxic metals from point-source anthropogenic sources like the Plant Barry ash pond.

3. Sampling strategy

To examine how changes in environmental conditions during different seasons impact the levels of toxic metals associated with coal ash in SS and SW and respective fluxes to the Mobile Bay Estuary, we conducted two sampling campaigns, one during the dry season (July–September 2021) and one during the rainy season (March–June 2022). To decipher the impact of storms on metal distribution in the area, we conducted an additional third sampling campaign on March 14, 2023, two days after a significant storm event which resulted in 46 mm precipitation from March 12 to March 13, 2023). Hereafter, we refer to it as the "post-flood" sampling event. Sampling campaign details are also presented in Table 1.

To estimate the magnitude of toxic metal contamination near Plant Barry's ash pond in the aqueous phase, we collected ambient river SW by submerging offboard a grab-sampling aid made entirely of PVC carrying an acid-cleaned 250 mL wide-mouth HDPE sampling bottle to avoid trace metal cross-contamination. For each season, up to 25 samples were collected in 250-m intervals for a 6.4 km total transect length (Fig. 1B, Table 1). In-situ water parameters, e.g., temperature, pH, conductivity, DO, were measured using a handheld YSI instrument. The collected ambient river water was filtered through a 0.45 μm PTFE filter. This fraction includes dissolved trace metals and colloids of <0.45 μm (Wen et al., 1997; Wen et al., 1999). Collected SW samples were stored on ice, transported to the UA Coastal Hydrogeology Laboratory, and placed in a refrigerator (at <6 °C) before further analyses.

To evaluate the spatial and seasonal distributions of SS and associated metal contents, we deployed Time-Integrated Mass Samplers (TIMS), as described in previous estuarine research (Elliott et al., 2017) (Fig. 1, Table 1). The inlet flow velocities of our TIMS were calculated following Elliott et al. (2017) and indicated that all river flow regimes during our study fall into an inlet flow range between 0.3 and 0.6 m/s. At this range, the TIMS captures over 93 % of the suspended sediments that flow through the tube with an average of 10.5–15 μm d50 particle sizes for marsh sediments and a higher average sediment particle size retention at higher inlet flow with an average of 9.58 to 13.3 d50 μm particle sizes, but an overall range of 0.1 to 200 μm. Based on these results, we assume at least a 93 % retention of SS and an average range of 9.5 to 16 μm d50 particle size. Previous studies examining fly ash particles report particle size distributions between 6.8 and 98 d50 μm with more fine-grained fly ash particles relating to higher toxic metal contents (Elliott et al., 2017; Lanzerstorfer, 2018). Therefore, SS and associated toxic metal fluxes reported here should be considered conservative estimates of the actual fluxes and are expected to capture the majority of ash particles sourced from Plant Barry's ash pond that may enter the Mobile River. Similar to research by Stewart (2020), the TIMS body was submerged about 0.46 m (1.5 ft) from the water surface and secured with metal ratchet straps during each deployment (Appendix A). Upon retrieving the TIMS from their deployment locations, we poured the sediment-water slurries into cleaned 20-L carboys and transported them to the Coastal Hydrogeology Laboratory at UA for further analysis.

Table 1
Summary of the sampling events conducted during this study, including sample type, collection date and duration, and tidal stage. For exact sampling locations, see the map in Fig. 1.

Sampling season	Sample type	Sample ID	Date of collection	Tidal conditions
Dry Season July–September 2021	SS	Dry TIMS-1 Dry TIMS-2 Dry TIMS-3 Dry TIMS-4 Dry TIMS-5	9/27/2021 (62 Days)	
	Surface Water	Dry SW-1-25	7/27/2021	Spring high tide
Wet Season March–June 2022	SS	Wet TIMS-1 Wet TIMS-2 Wet TIMS-3 Wet TIMS-4	6/16/2022 (91 Days)	
	Surface Water	Wet SW-1-25	3/17/2022	Ebbing low tide
Post-flood sampling March 2023	Surface Water	Flood SW-1 - 25	3/14/2023	Spring high tide

The five TIMS units were deployed at the same locations across two sampling campaigns for a collection period between 60 and 90 days (Table 1), which is also the field practice elsewhere (Elliott et al., 2017; Stewart, 2020). Additionally, we strategically deployed each TIMS in five sections along the 6-km river stretch to capture the contributions of three significant end members. Following an upstream-downstream trajectory (Fig. 1B), these endmembers include water from (i) upstream Mobile River contribution (TIMS-1), (ii) the Pond-River section of the transect with suspected surface runoff and groundwater contributions from the Plant Barry ash pond (TIMS-2 and TIMS-3), and (iii) the outlet of Plant Barry's Sister's Creek wastewater discharge cooling channel (TIMS-4). We assumed that the SS metal composition at TIMS-5 is cumulative upstream of these three end members (Callaway et al., 2018).

The degree of metal contamination within the sample transect was evaluated through multiple established metal factor indices, including the geochemical enrichment factor (EF), geoaccumulation index (I_{geo}), contamination factor (CF), and pollution load index (PLI), and compared by season (Paul et al., 2021). Arsenic and Cd, common toxic metals associated with coal ash, were selected for illustration of these metal contamination indices based on their high mobility in aqueous environments, high content in industrial wastes, and documented history of

toxicity in aqueous environments following desorption from coal ash (Smedley and Kinniburgh, 2002; Galunin et al., 2014; Gorny et al., 2015; Wang et al., 2023). Metal contents in SS collected by TIMS units were utilized in a multivariate mixing model to assess endmember contributions during the dry season sampling transect. Finally, statistical analyses, including Spearman r^2 correlation and multivariate PCA, were used to identify the significance of environmental conditions, water quality parameters, and source contributions of the major and toxic trace metals analyzed.

4. Analytical methods

The collected TIMS sediment-water slurries in the lab were poured into 50-mL centrifuge tubes and centrifuged at 4000 rpm for 5 min to separate particles from water. Following decanting the water from the centrifuge tubes, TIMS sample residues were removed from containers using cleaned plastic forceps and air-dried within a fume hood for 24–48 h before being weighed at 0.0001 g precision with a Mettler AT261 DeltaRange scale. TIMS units collected a range of 0.7 to 22.5 g of dried sediment between the dry and wet seasons (Supplementary Tables). Dried SS samples were ground using an agate mortar and pestle for homogenization. The mortar and pestle were cleaned between samples with deionized water and acetone. Triplicates of 0.5 g, except for wet season TIMS-4 due to insufficient sediment, of the collected dried TIMS samples were microwave-digested with 10 mL of Nitric acid 67–70 % (ARISTAR® PLUS for trace metal analysis) in sealed acid cleaned and air-dried Teflon containers. The samples were digested in an Anton-Paar Multiwave 5000 microwave digestion system at 190 °C for 20 min. Solutes following microwave digestion were decanted by a syringe, filtered through 0.45 μm, into ICP-OES sample tubes, and diluted using dilution factors of 20 or 100 (DF:20, DF:100) with 2 % HNO_3. This partial digestion method aims at mobilizing only the sediment-bound metals' "environmentally available" portion (Melaku et al., 2005; Perez-Santana et al., 2007). Additional analyses for direct identification of coal ash particles, including XRD mineralogical analysis, SEM, and Atom Spectrometry, were considered prior to sampling but were not performed due to the lack of sufficient collected material (Xu et al., 2014; Zhu et al., 2024).

The SW samples were filtered through 0.45 μm PTFE membrane filters (Pall Laboratory) into acid-cleaned 50-mL centrifuge tubes. At this filter pore size, the evaluated major and trace metal concentrations are attributed to the dissolved and colloidal fractions (Khaska et al., 2015). Before analyses, filtered SW samples were prepared with 0.2 mL of 2 % HNO_3 added to a total of 10 mL in sterilized sample tubes.

Metal contents in SS and metal concentrations from filtered SW samples were analyzed by an Agilent 5800 ICP-OES equipped with an SPS4 autosampler for Al, B, Ba, Be, Ca, Cd, Co, Cr, Cu, Fe, Mg, Mn, Ni, Pb, Se, Sr, Ti, Tl, V, Zn, Si, K, and Na following EPA Methods 3051 A and 200.8 for TIMS and SW samples, respectively. Six calibration standards ranged from 0.05 to 20 ppm (0.00, 0.05, 0.10, 1.0, 10, 20 ppm), and laboratory blanks were used to determine the detection limits of individual metals. Using our instrumentation, the detection limits for As, Cd, Co, Cr, Pb, and Mn in the wet season SS samples were 0.05, 0.02, 0.04, 0.04, 0.02, and 0.05 ppm, respectively. All metal DLs are provided in Supplementary Tables.

5. Sediment flux assessments, mixing model analysis, and end member contributions

To evaluate the SS fluxes at each TIMS location within the 6-km river section (Fig. 1B), we used an equation based on a relationship between SS metal content and the associated season-specific discharge of the Mobile River:

$$F_{TIMS} = SSC_{(in-situ)} \times Q_R \quad (1)$$

where: F_{TIMS} is the average sediment flux (g/s) for the respective $TIMS_i$, $SSC_{(in\text{-}situ)}$ is the average SS concentration (g/m^3) within each TIMS unit, and Q_R is the average Mobile River discharge (m^3/s) at the nearest USGS river gage, i.e., Mile 31.0 stream gage in Bucks AL for the duration of the deployment. The SS concentrations of each TIMS were determined by dividing the total mass of sediment collected each season by the volume of water processed during each deployment's duration, defined by ambient stream flow velocity within the TIMS (Elliott et al., 2017; Stewart, 2020).

To calculate metal fluxes from each season at each TIMS location, we first multiply the associated metal content (mg/kg) by the total amount of sediment (g) collected by the TIMS to obtain mass. The estimated mass (g) of each metal is then divided by the total sampled volume (m^3) of water to obtain mass metal concentrations (g/m^3). Finally, the individual seasonal metal fluxes (g/s) are calculated by multiplying by the USGS Mobile River Mile 31.0 river discharge (m^3/s) for their respective seasonal deployment.

To evaluate the total suspended sediment flux contributions (F_{total}) within the sampled river transect, we constructed a mass-balance source model based on the three end members:

$$F_{total} = F_R + F_{PR} + F_{DC} \quad (2)$$

where F_R represents the upstream Mobile River, F_{PR} is the ash pond-adjacent river section, and F_{DC} is the contribution from the ash pond discharge channel. As mentioned in section 3 Sampling strategy, we assumed that the composition of the surface water and the SS collected at TIMS-5, is the result of mixing three metals' sources, i.e., end members, namely (i) the upstream Mobile River (R) represented by TIMS-1, (ii) the ash-pond area adjacent river (PR) collected by samplers TIMS-2 and TIMS-3, and (iii) the Sister's Creek discharge channel (DC) collected by sampler TIMS-4.

Using these endmembers and metal content from each TIMS1–4 unit, we further constructed a multivariate mixing model following Gellis et al. (2009) to assess the percentage contribution of each TIMS location to the downstream TIMS-5 sediment composition (Gellis et al., 2009). This model utilizes selected inputs of a tracer source metal contents (upstream) to match downstream mix tracer contents at TIMS-5. The model also accounts for associated variances. In our study, the number of sources is based on the definitions in Eq. 2. The overall sediment contribution to TIMS-5 is calculated by adding the model-predicted percent contribution from each defined source. The Gellis Landwehr model is provided in Eq. 3:

$$T = \left(\frac{1}{n}\right)\sum_{i=1}^{n}\left|C_i - \sum_{j=1}^{m} X_j S_{ji}\right| \Big/ \sqrt{\sum_{j=1}^{m} X_j^2 \left(VAR_{ij}/m_j\right)} \quad (3)$$

where: *T* is the total contribution, **Ci** is the metal's individual contents (i) in the downstream outflow TIMS-5, **Sij** is the metal content in a specific TIMS source as (j), **Xj** is the percentage contribution from each TIMS source (j), **VARij** is the variance of the measured values of metal contents (i) in each TIMS source (j), **mj** is the total number of samples for an individual TIMS source, m is the number of metals used in the model, and m is the number of sediment sources (3). The Gellis Landwehr model was chosen because of its successful performance in similar research by Stewart (2020), who used metal contents and sediment properties as tracers to determine sediment source contributions within the Mobile Tensaw Delta. Under the parameters described in Eq. 3, the model can be mathematically solved without any initial assumption of percentage contribution from each TIMS source. Twenty iterations were performed using this method, and results were averaged to obtain each source's percentage contribution to the downstream TIMS-5 sediments.

6. Metals pollution evaluations

To evaluate possible metal pollution in the collected SS, we used four different contamination indices (Table 2), including the (i) geochemical enrichment factor (EF), (ii) geoaccumulation index (I_{geo}), (iii) contamination factor (CF), and (iv) pollution load index (PLI)(Zhang and Liu, 2002; Birch and Olmos, 2008; Islam et al., 2015). These indices are utilized to determine anthropogenic and non-crustal sources of metals of interest. The formulas for these equations, variables, and threshold classifications are provided in Table 2, as described by Paul et al. (2021).

In all cases, for background levels we used sediment metal content reported in two studies: (1) a 1991 EPA study at the Mobile River upstream of Plant Barry and (2) a 2018 Mobile Bay Keepers report for additional metal content not found in the first report.

In these evaluations, C_m is the concentration of the metal of interest, and B_m is the background metal concentration; C_{Fe} and B_{Fe} represent Fe contents for each sample of interest and background sample Fe contents, respectively. CF is the contamination factor of metals 1 through "n", where "n" is the number of metals analyzed (Zhang and Liu, 2002; Birch and Olmos, 2008; Islam et al., 2015).

We used the geochemical Fe-EF to evaluate the magnitude of metal contamination at each TIMS location (Buat-Menard and Chesselet, 1979; Villaescusa-Celaya et al., 2000; Barbieri, 2016). While many techniques and methods have been established for determining metal enrichment factors, Fe-normalization was preferred for this study instead of Al, for example, because of iron's relatively higher content in soil and sediments compared to contaminant trace amounts (e.g., Co, As, Cr, Ni, etc.) and hence its content is less affected by possible contamination from anthropogenic sources compared to aluminosilicates and trace metals (Almasoud et al., 2015; Paul et al., 2021). The TIMS-1 location was collected about 1.1 km upstream from Plant Barry, representing a "non-contaminated/background levels" sediment. Fe-normalized EF values above 1.5 indicate an external addition of metals from anthropogenic non-point sources, while values below 1.5 indicate natural accumulation (Barbieri, 2016; Paul et al., 2021).

We also used a sediment geo-accumulation index (I_{geo}) to evaluate the degree of accumulation through time and distance (Martínez and Poleto, 2014; Haris et al., 2017). The range of possible I_{geo} thresholds is between 0 and 5, where $I_{geo} = 0$ indicates no contamination, while $I_{geo} \geq 5$, indicates extreme metal contamination (Yaqin et al., 2008). The 1.5 value in the denominator of the I_{geo} equation accounts for the natural fluctuations of metal sources within sediments (Table 2) (Yaqin et al., 2008).

Finally, the contamination factor (CF) and pollution load index (PLI) were utilized to calculate individual and standardized toxicity of each TIMS sample for the 13 metals analyzed (Al, As, Ba, Ca, Cr, Cu, Fe, Mg, Mn, Ni, Se, Zn, and K) which have appropriate background content (Table 2). The CF for each metal represents the ratio of measured metal content versus the unaffected, i.e., background sample content. The PLI measures the total toxicity of the sediments, and it is determined by adding all CFs and calculating the average. PLI values of 0 indicate no toxic pollution, 0–1 indicates a baseline pollution level, and values >1 represent progressive sediment deterioration with metal contamination.

7. Sources of metal contamination variations: Statistical analyses

Previous research has used PCA to investigate associations between metal content and sediment grain size fractions, organic matter, and physical properties concerning anthropogenic inputs (Loska and Wiechuła, 2003; Idris, 2008; Hsu et al., 2016). We utilized PCA to cluster SS and SW samples based on observed environmental parameters. Correlation between environmental parameters was analyzed using Spearman correlation, and only correlations with p-values <0.05 were considered for analysis and discussion. All statistical analyses were implemented in R version 4.4.1 using the vegan package version 2.6–6.1 and corrplot version 0.94 (Oksanen et al., 2013).

8. Results

8.1. Temporal and spatial distributions of surface water physical parameters

Conductivity in surface waters varied significantly between sampling seasons (Fig. 2A), with the lowest average conductivity observed during the wet season (80–97 μS/cm) followed by the dry season (100–127 μS/cm). The surface water conductivity during the post-flood sampling event was two times higher compared to the dry season. It was also the least varied across all sampling events (227–232 μS/cm), with the highest conductivity (232.0 μs/cm) measured at the Sister's Creek discharge channel outlet (SW21 to 23, near TIMS-4), see Appendix B. A closer inspection of this spatial distribution (Fig. 2A) revealed that while the conductivity measured at SW23 was only 1.6 % higher than the average within the post-flood sampling event, it was 37 % higher than

Table 2
Modified list of metal contamination factor formulae and classification from Paul et al. (2021) describing sediment contamination levels.

Factor	Formula	Classification categories	Specifics
Fe- Enrichment Factor (EF)	$\frac{\frac{C_m}{C_{Fe}}}{\frac{B_m}{B_{Fe}}}$	<1.5 no anthropogenic modification 1.5–3 minor anthropogenic modification 3–5 moderate anthropogenic modification 5–10 severe anthropogenic modification	Used to evaluate the magnitude of metal contamination by normalizing to a major element
Geoaccumulation Index (I_{geo})	$Log_2\left(\frac{C_m}{1.5*B_m}\right)$	<0 no contamination 0–1 none to moderate contamination 1–2 moderate contamination 2–3 moderate to heavy contamination 3–4 heavy contamination 4–5 heavy to extreme contamination >5 extreme contamination	Utilized to assess the accumulation of metals from anthropogenic and non-crustal sources
Contamination Factor (CF)	$\frac{C_m}{B_m}$	<1 low degree of contamination 1–3 moderate degree of contamination 3–6 considerable degrees of contamination >6 very high degree of contamination	Calculates toxicity from the ratio of individual metals and their background concentrations
Pollution load Index (PLI)	$(CF1*CF2*CF3*\ldots*CF_n)^{\frac{1}{n}}$	0 no pollution 0–1 baseline pollutants >1 progressive deterioration	Determines total toxicity by standardizing the contamination factor of all metals

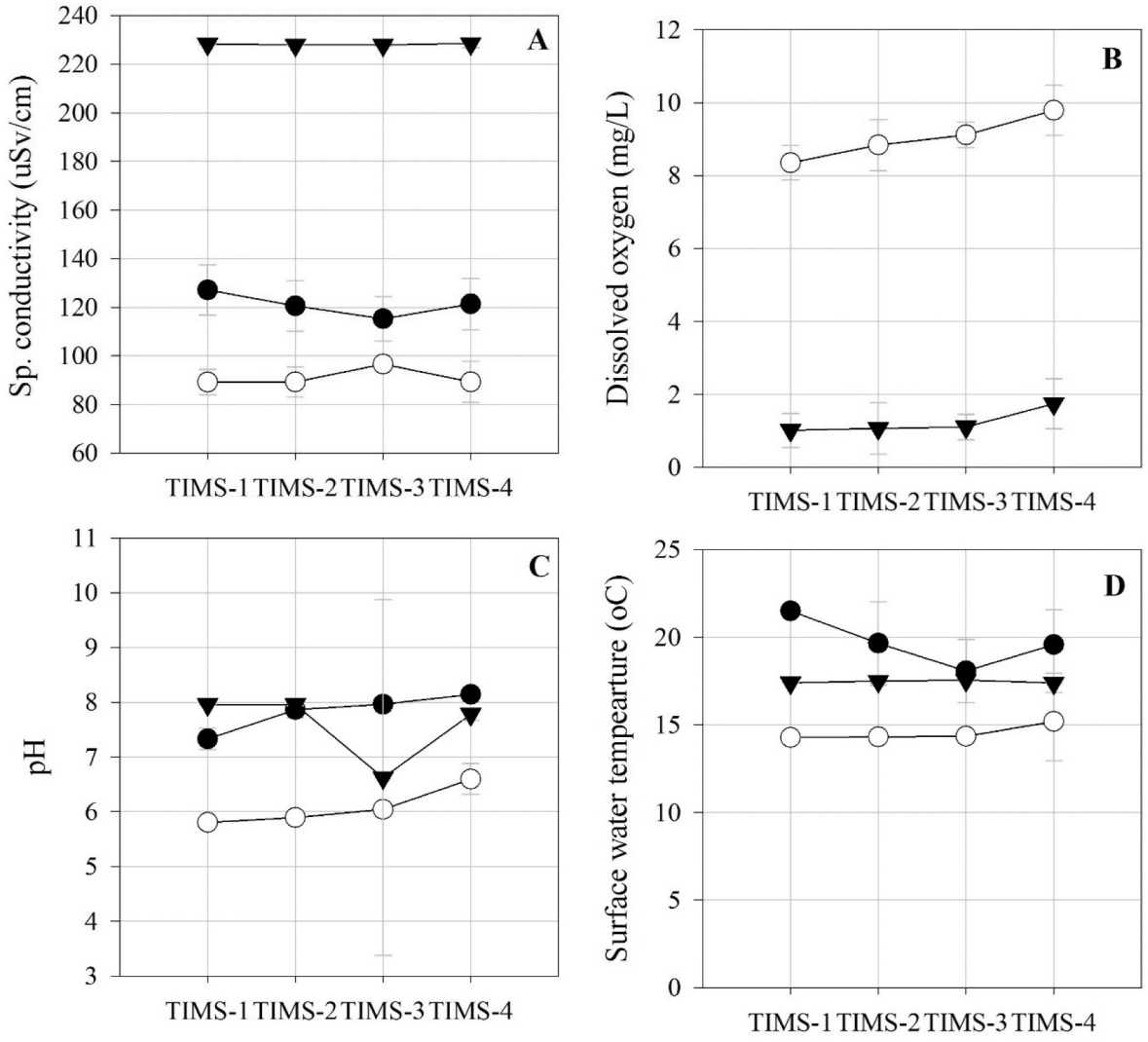

Fig. 2. (A) Spatial conductivity (μS/cm), (B) dissolved oxygen (mg/L), (C) pH, and (D) surface water temperature (°C) distributions during the sampling events representative of the dry season (black circles), wet season (white circles), and post-flood conditions (black triangles). Values are representative of physical property averages of surface water samples near associated TIMS sampler positions for comparison.

the average conductivity across all other seasons during our study. Overall, spatially, during the dry season, we observed higher conductivity in the transect locations upstream (SW1 to 9, near TIMS-1) and downstream of the ash pond (SW18 to 25, near TIMS-3&4), and lower conductivity adjacent to the perimeter of the ash pond (SW 10 to 17, near TIMS-3) (Fig. 2A**)**. We suggest that these conductivity results are due to a combination of lower precipitation and streamflow, which would allow saline water from Mobile Bay to propagate farther upstream. Other factors, such as the spring high tide during sampling, shallower water depth, and accumulated river channel sediments, exacerbated these effects during the dry season. In contrast, the wet season SW samples were collected during an ebbing tide and captured more recent precipitation (105 mm within 10 days), which resulted in lower conductivity in the area and smoothing of spatial variations (Fig. 2A).

We collected reliable dissolved oxygen (DO) data during two of the three campaigns, i.e., the wet season and post-flood sampling event. Our observations revealed a large seasonal DO variability (Fig. 2B). The surface water was more oxygenated during high flow conditions (DO 7.73–10.37 mg/L) than during the post-flood sampling event (DO 0.9–2.65 mg/L). These alarmingly low DO levels, below the 2–3 mg/L threshold, throughout the transect indicate hypoxia during the post-flood sampling event were somewhat surprising for us. However, such hypoxic conditions, referred to as “blackwater events”, often develop in the aftermath of flood events in coastal plains at relatively high temperatures (Kerr et al., 2013). Following flood events, rivers carry washed-out plants and various organic matter, which causes bacteria to break down and consume oxygen. Lower oxygen levels affect aquatic life, the geochemistry of waters, and associated metal concentrations. Nevertheless, spatially, during both sampling events, we observed significant increases in DO (by 14 and 72 %, respectively) past the southern edge of the ash pond and at the Sister’s Creek discharge channel and downstream from SW20 to 25 near TIMS-4 and TIMS-5 (Fig. 2B).

River water pH varied moderately (7.27 ± 1.0, $n = 73$) throughout the sampling seasons (Fig. 2C). The highest temporal variations in pH were observed during the dry season when the river contribution was the lowest. This resulted in proportionally more significant impacts on the discharge channel and Mobile Bay saltwater propagation (Fig. 2C). During the wet season, pH was below neutral, varying between 5.75 and 6.93, while in the dry season, it was slightly above neutral but generally in the alkaline range (7.01 to 8.30). During the post-flood sampling event, pH was also in the neutral range and remarkably stable with 1.2 % variations. We attribute the lower average pH across the entire transect during the wet season to higher precipitation before sampling,

which is generally more acidic. Notably, pH increased farther downstream from sampling stations SW20 to 25 during the dry and wet seasons (Fig. 2C). We attributed the increase in pH to mixing river water with water from Mobile Bay, which has a characteristically marine component with alkaline pH. On the other hand, the post-flood pH spatial distribution (7.57–7.67) had the opposite trend, with slightly lower pH near the Sister's Creek discharge (Fig. 2C).

Temporally, the surface water temperature was relatively uniform (17.2 ± 2.6 °C) throughout all three sampling events (dry 19.7 ± 2.1 °C, wet 14.5 ± 1.1 °C, and post-flood 17.5 ± 0.3 °C), except at particular "hot spot" locations (Fig. 2D). For example, the upstream dry season temperatures SW1 to 11 were distinctly higher from (21.4 ± 0.3 °C), then decreased by >15 % around the perimeter of the ash pond between SW12 and 22 (17.7 ± 1.5 °C) and increased again between SW22 and 25 (21.3 ± 0.3 °C). We attribute these changes to the variable underlying river channel depth, increased stream flow along the river bend, and boating activity mixing surface waters with the water column below during the dry season. We also suggest that the significant increase in temperature, i.e., "a hot spot" (from 18.1 to 21 °C) observed at SW20 and SW21 near TIMS-4 is most likely the result of hotter wastewater contributions from the Sister's Creek discharge channel (Fig. 1). We observed an increase in water temperature near Sister's Creek (SW21) in every sampling event, with a 5 °C increase during the wet season (14.3 °C average) and less pronounced increases during the dry season and post-flood sampling event (Appendix B). These SW temperature variations support the notion that the ash pond and discharge channel alter the estuarine environment with their discharge along the downstream section of the river stretch.

8.2. Temporal and spatial distributions of dissolved major naturally occurring and toxic metal fluxes

Dissolved metal fluxes near the locations where the TIMS samplers were deployed were calculated by multiplying the average surface water metal concentrations (SW_i) of the closest sampling sites and the river discharge during the three sampling events. Fig. 3 shows the temporal and spatial variability of Fe (Fig. 3A) as representative of naturally occurring metals such as Al, Fe, Ca, Mg, and Si compared to dissolved As (Fig. 3B) and Cd (Fig. 3C) fluxes, as representative of the dissolved toxic metal fluxes (e.g., As, Cd, Co, Ni, V, Ti, and Li) in the study area.

Iron and most naturally occurring dissolved metal fluxes displayed a specific spatial pattern, with higher fluxes around TIMS-2&4 compared to TIMS-1&3 sites (Fig. 3B, (Fig. 3). Also, except for Al, all other dissolved major metal fluxes were the highest during the post-flood sampling campaign and lowest during the dry season. Temporally, we observed a significantly broader range in dissolved toxic metal fluxes. For example, As, Cd, and V were not detectable (or at very low concentrations) in surface water during the post-flood sampling, while during the dry season, we observed exceptionally high toxic metal fluxes, for example Cd dissolved fluxes were between 130 and 720 times higher in the dry season compared to the wet season (Fig. 3C). This anomaly was observed near TIMS-2 (Fig. 3A). Similarly, we observed an accumulation pattern of Ni dissolved fluxes from upstream to downstream, with an extreme flux calculated near TIMS-4 reaching 50 times higher than the same location during the wet season. Other toxic metal fluxes, e.g., Li, V dissolved fluxes, showed apparent accumulation downstream (TIMS-1 to 4) during the wet and post-flood sampling events (Appendix D).

In summary, we observed relatively high toxic metal fluxes with hot spots for certain metals, i.e., Cd, Co, Cu, Mn, Ni, etc., at intermediate SW12 to SW18 locations. Higher river discharge was not always associated with higher metal fluxes. Results from this study show that the elevated dissolved Cd fluxes during the dry season were the result of high levels of Cd in surface water (0.3 to 0.4 mg/L) rather than the magnitude of the river discharge (957 m^3/s) during collection. The average Cd flux through the river section was 2876 kg/day during the dry season (>260 times fluxes recorded during the wet season), with the highest detected toxic metal flux located near TIMS-2 (Fig. 3C). Conversely, Cd concentrations in surface water were below detection during the post-flood sampling event (Appendix D4).

Major metal fluxes also revealed an accumulation pattern (Fig. 3A), whereas associated dissolved fluxes were lowest during the dry season when the river discharge was lowest. On the other hand, we calculated the highest dissolved major metal (e.g., Fe) fluxes during the post-flood hydrological regime. These exceeded 1.5 times those during the dry season and were 40 % higher during the wet season. These trends confirmed the notion that the major metal fluxes were controlled by the river discharge and the changes in the environmental condition (higher conductivity, low DO, Fig. 2A&B) during the post-flood environmental conditions.

8.3. Spatial and temporal variability of total SS and associated metal fluxes

Using Eq. 1, we calculated SS fluxes at each TIMS location within our study site (Fig. 4A). Although the river discharge was about 60 % lower during the dry season (Fig. 1A), the SS fluxes were close to four times higher during that season compared to the wet season (Fig. 4A). However, the overall pattern was the same during both seasons, regardless of the magnitude of the SS flux. Metals associated with riverbed erosion, i.e., Fe, Al, etc., were higher overall during the dry season compared to the wet season, and all showed a decreasing trend from upstream to

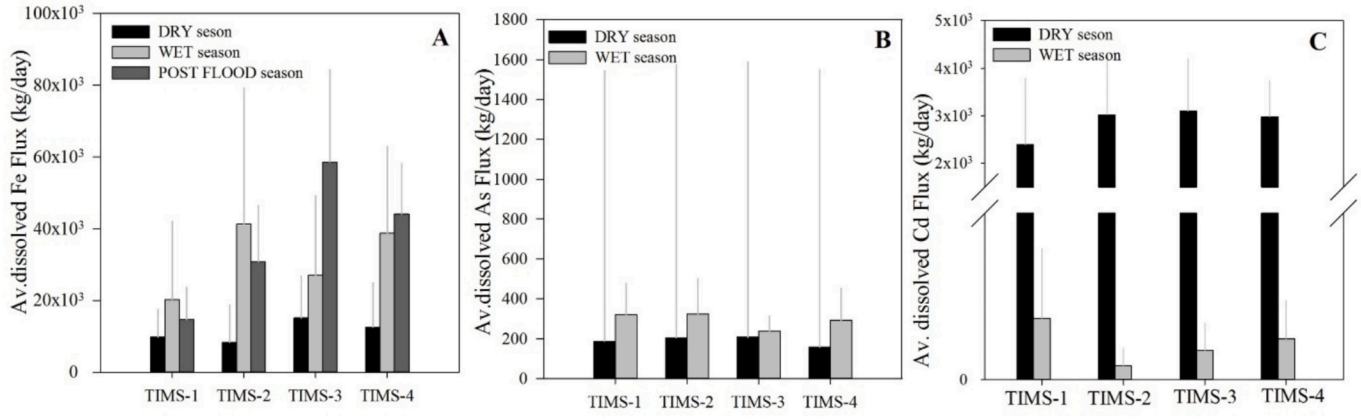

Fig. 3. Average metal concentration fluxes near TIMS positions of (A) Fe, (B) As, and (C) Cd, respectively. Black columns represent the dry season, light grey columns represent the wet season, and dark grey columns represent the post-flood sampling event.

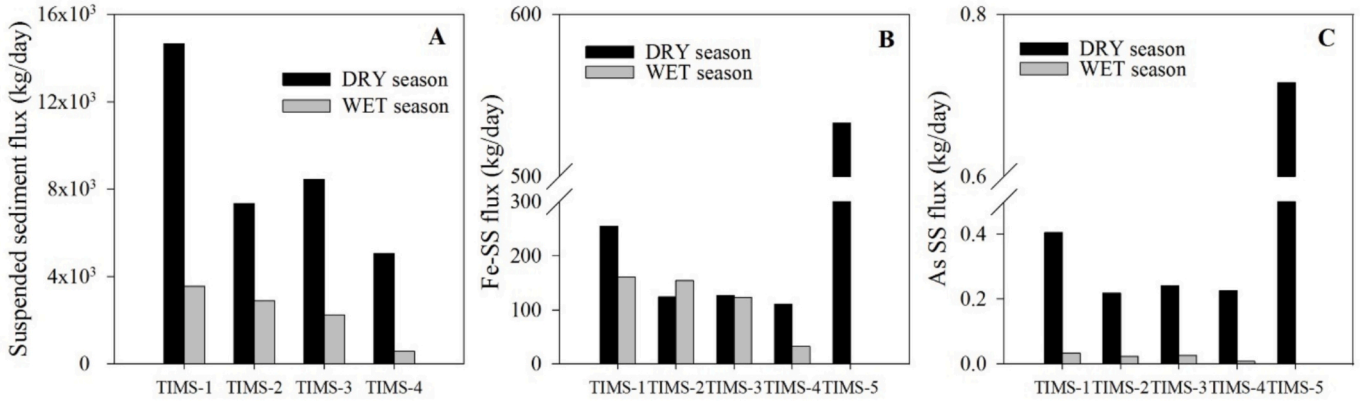

Fig. 4. (A) Suspended sediment fluxes and SS-metal fluxes of Fe (B) and As (C) by TIMS sampler position (kg/day). Black columns represent dry season TIMS samplers, and grey columns represent wet season TIMS samplers. Except for Fe at TIMS-2, both the sediment and SS-metal fluxes were higher across all TIMS positions during the dry season. The SS-As fluxes were significantly higher during the dry season (C).

downstream (Fig. 4B). However, we observed the reverse seasonal patterns in the distribution of most toxic metal fluxes, e.g., As (Fig. 4C). Furthermore, SS-As fluxes were one order of magnitude higher during the dry season (av. 0.4 ± 0.3 kg As/day) compared to the wet sampling event (av. 0.02 ± 0.01 kg As/day). Arsenic is a metal associated with potential contaminations from the Barry Power Plant. SS-As fluxes at TIMS-4 were 30 times higher during the dry season, and the TIMS-5 site showed even higher As-SS flux (0.9 kg As/day). Other metals, such as Pb, Cr, Co, Ni, and Ti, were also the highest at TIMS-4, some of these up to 2–3 times higher than the average fluxes (Appendix C&D).

8.4. Relative metal contamination levels in SS

When comparing the temporal variability of Fe-normalized EF, we found that all naturally occurring and toxic metals were considered below the threshold of anthropogenic contamination (Fe-EF <1.5) during the wet season. However, Fe-EFs were up to four times higher during the dry season across the transect, specifically for toxic metals such as As and Cd (Fig. 5A&B). When comparing our results to calculated Fe-EF from previous research by the EPA in 1991 and SELC sampling done in 2016, we found both the dry season and wet season metal Fe-EFs exceeded all comparable historical records and averaged 2.25 2.86 across the transect (Table 1 in Appendix C). Specifically, the highest individual Fe-EF of As (5.59) and Cd was at TIMS-4, indicating severe anthropogenic modification (Table 3, Fig. 5).

Similarly, the calculated geoaccumulation index (I_{geo}) described in Table 3 indicated that As and Cd were in moderate (1–3) to high (>3) contamination levels across the entire sampling transect during the dry season, with a maximum of 2.54 for As and 3.22 for Cd at TIMS-4, respectively (Table 2 in Appendix C). On average, most other metals during the dry season had <1 I_{geo}. However, we also observed gradual increased I_{geo} of major metal Al, Ba, and trace metal Co, Cr, and Ni up to moderate contamination (1–3) at TIMS-4, suggesting geoaccumulation (Table 2 in Appendix C). Zinc was the only metal during the dry season with moderate contamination (I_{geo} = 1.2 to 2.7) but lower I_{geo} indices downstream at TIMS-2 through TIMS-5 than upstream TIMS-1.

When examining the contamination factor (CF), as to be expected from sediment metal contents, we calculated maximum levels of As and Cd at TIMS-4 during the dry season at 8.8 and 14, respectively, which is classified as a very high degree of contamination (>6) (Table 3 in Appendix C). We found that, excluding Co, all major and trace metals exceeded a moderate degree of contamination (>1 CF) on average during the wet season. Toxic metals such Cr, Cu, and Ni exceeded a considerable degree of contamination (3–6) at the TIMS-2 position (Table 3 in Appendix C).

Finally, when using the cumulative PLI of these CF indices, we observed progressive worsening of the sediment contamination (PLI > 1) across all TIMS positions during both the wet and dry seasons. We found both the lowest PLI at TIMS-3 (1.76) and the highest PLI at TIMS-4 during the dry season (3.36) (Table 3 in Appendix C). The PLI at each

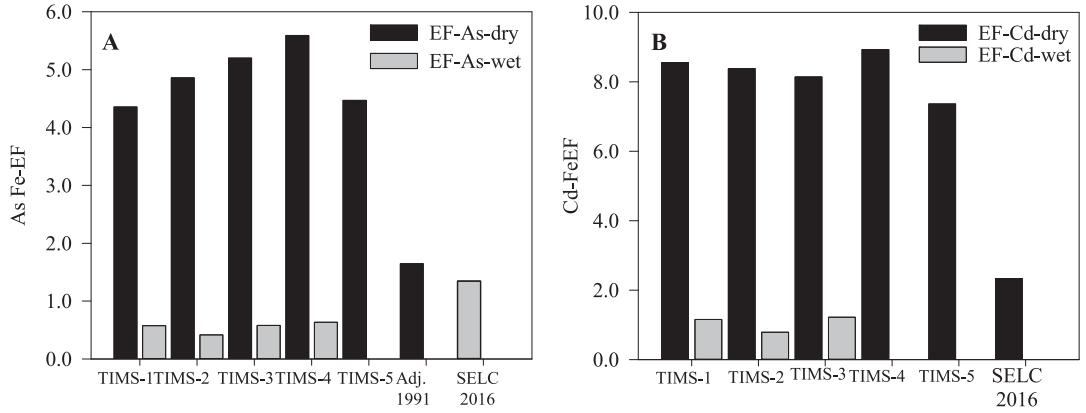

Fig. 5. Arsenic (As) and cadmium (Cd) iron Enrichment factor (Fe-EF) estimates across the five TIMS locations in the study site. The black columns represent data from the dry season, while the grey columns represent data from the wet season. The sediment sample from EPA 1991, located adjacent to the river, and the SELC 2016 sediment sample are included for comparison and are color-coded based on their respective environmental conditions. The Fe-enrichment factors for As and Cd during the dry season were significantly higher across all sampling locations, with the TIMS-4 position near the discharge channel exhibiting the highest enrichment factor of 8.93, indicating severe anthropogenic impact.

TIMS position during the wet season is higher than the counterpart dry season at every location except at TIMS-4, which illustrates the increase in metals from the ash pond perimeter through surface runoff while diluting the contribution of toxic metal contents at the discharge channel with higher river discharge (Table 3 in Appendix C).

8.5. End-member contributions: Mixing model results

Using Eq. 3 and endmember definitions described in Eq. 2, the Gellis Landwhear mixing model was run twenty times with different initial contributions from each TIMS position during the dry season and subsequently averaged (Fig. 6, Supplemental Tables). Since the TIMS-5 unit was not recovered following the wet season sampling deployment, we report only findings from the dry season, which, nevertheless, are explicit and informative.

Based on the averaged mixing model results, the ash pond adjacent river section of the transect (TIMS-2 and TIMS-3) contributes 81.2 % of the total sediment composition to the downstream TIMS-5 endmember, with the discharge channel TIMS-4 (11.7 %) and upstream TIMS-1 (7.1 %) contributing sediments in minor amounts (Fig. 6). These mixing model results indicate that most of the SS collected downstream at TIMS-5 during the dry season originates from the river section closest to the ash pond perimeter. While the SS from TIMS-4 position exhibited high trace metal content, metal fluxes, and the highest metal contamination indices during the dry season, the sediment contribution from this position is significantly lower than that from the intermediate TIMS-2 and 3 positions (Fig. 6).

8.6. Statistical analysis of environmental water parameters, metal concentrations and SS metal contents

The results from statistical analysis, i.e., PCA and Spearman correlations using metal concentrations in surface water and physical properties across all three sampling events are provided in Fig. 7. Principal component analyses of surface water samples indicated that approximately 54 % of the total variation could be explained with two components. The first component explaining 33.6 % of the total variance is primarily associated with in-situ surface water conditions split into two categories of post-flood water parameters against non-flooding periods (i.e., the post-flood and wet vs. dry seasons). The unique post-flooding samples cluster correlated with elevated conductivity and pH levels and, to a lesser degree, temperature (Fig. 7A). The second component, PC2, accounts for 20.5 % of the variability in metal concentrations in surface water and is strongly linked to Al, Fe, Ca, and Ba concentrations and negatively with sampling depth variations. Spearman correlation analysis further supports the co-occurrence of Al and Fe across all samples, revealing a robust positive correlation between the two metals ($\rho = 0.89$, $p = 0.05$) (Fig. 7B). When inspecting other Spearman correlations across all three sampling campaigns, we identified strong positive correlations between other major metal-Si and metal-metal pairs, including Na—Si ($\rho = 0.74$, $p = 0.05$), Na—Mg ($\rho = 0.90$, $p = 0.05$), Mg—Si ($\rho = 0.83$, $p = 0.05$), and Ba—Ca ($\rho = 0.85$, $p = 0.05$) (Fig. 7B). As demonstrated in the examples already described, these relationships suggest that the elements originate from a common geochemical sources and co-transport mechanisms or are involved in forming complexes and colloids in the water with Si.

PCA analysis of metal contents associated with SS samples shows two distinct sample clusters from the dry and wet sampling events. This clustering explains 82.3 % of the total variance (Fig. 8A). The first component, PC1, explains 60.1 % of the total variance and has a negative association with many metal contents, including Al, Be, Cr, Fe, Mg, and Pb. The second component, PC2, accounting for 22 % variation, is explained by the concurrent spatial increase of As, B, Ba, Mn, Ni, and Ti in SS collected by TIMS-4 near the Sister's Creek discharge channel (Fig. 8A). However, despite the highest Cd content observed at the TIMS-4 location (4.2 mg/kg), this toxic metal had no significant positive correlation with similar coal-associated metals such as As and Ti. We attribute this disparity to the significantly lower Cd content from TIMS-1 through TIMS-4 (Appendix A). While Spearman correlations of suspended sediment-associated metals during the dry season were not as strong as during the wet season, some significant correlations are worth mentioning (Fig. 8B). For example, Al, Cd, Cr, Mg, Pb, and Se all surpassed correlations of $\rho = 0.8$ ($p = 0.05$).

9. Discussion

9.1. Drivers of the magnitude of dissolved metals and associated fluxes

Based on our study, three main factors affected the levels of dissolved metals in the study site, including (i) seasonality in the river flow

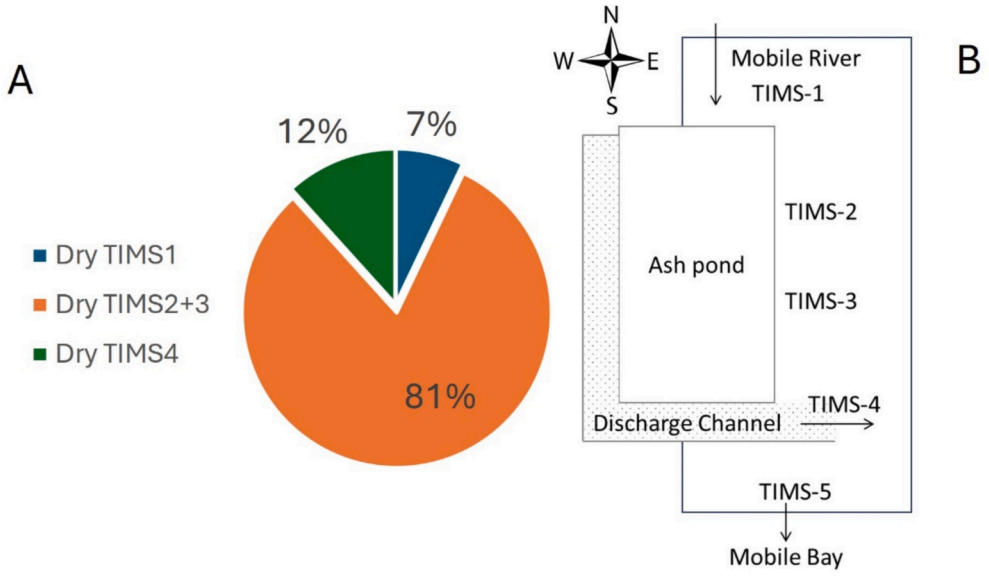

Fig. 6. Gellis Landwhear mixing model results for the dry season (A) and TIMS suspended sediments endmember configuration diagram (B). The sediments collected by TIMS-2 and 3 near the Plant Barry ash pond contribute to 81.2 % of the total sediment metal composition at the downstream TIMS-5 based on selected metal content tracers utilized. The upstream TIMS-1 and discharge channel TIMS-4 contribute 7.1 % and 11.7 %, respectively.

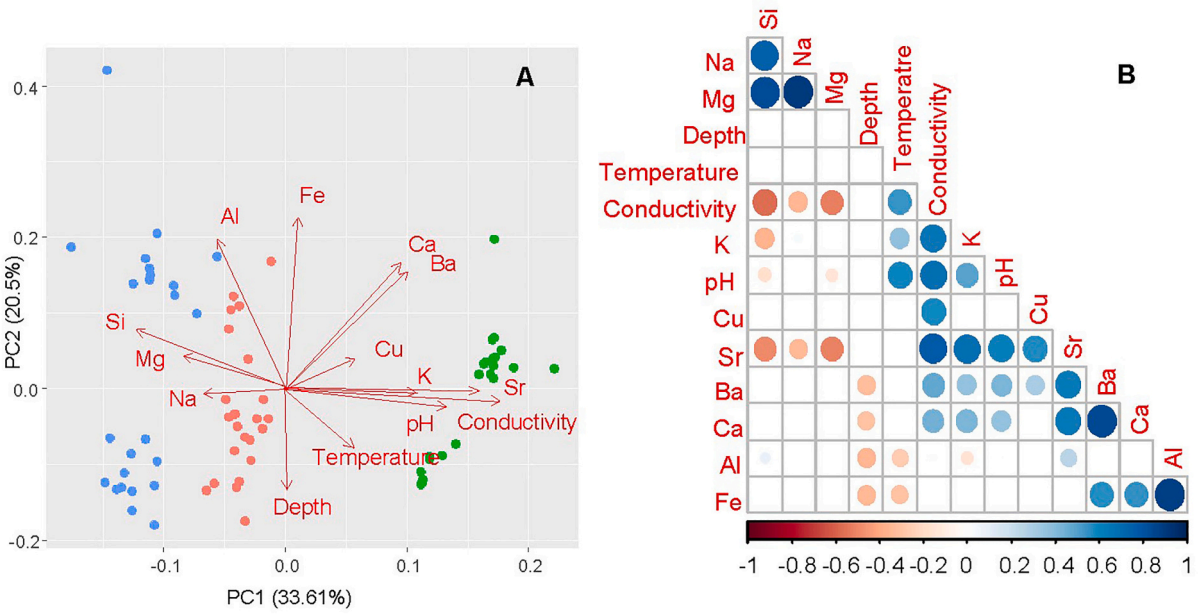

Fig. 7. (A) Principal Component Analyses (PCA) results based on metal concentration and environmental data for surface water samples: red circles represent dry season samples, blue circles represent wet season samples, and green circles represent the post-flood event samples. (B) Correlation matrix of dissolved metal concentrations and environmental data; blue circles indicate high positive correlation and red circles indicate high negative correlation.

regime, (ii) resuspension due to erosion at shallow river stretches, and (iii) discharge from the Plant Barry's cooling channel. PCA show that seasonality, i.e., magnitude of river discharge, was the primary control for the variance of the surface water physical properties (conductivity and pH) and major and trace metal concentrations (Fig. 7A). The different metals' responses to these drivers and the induced water quality changes also depended on their specific geochemical properties. Sampling depth and associated erosion were the second most important factors (Fig. 7A). Positive temperature anomalies near the discharge channel of Plant Barry were also indicators of higher dissolution rates and an overall increase in metal concentrations across all three sampling events.

PCA results indicated that samples collected during post-flood conditions were statistically different from those in the dry and wet seasons (Fig. 7A). On average, major metals, such as Na, Ca, and Ba, and toxic metals, such as Co, Ni, and Cu, were up to two times higher during the post-flood sampling event compared to transect averages during the wet and dry seasons (Appendix B). We suggest that sediment resuspension and increased runoff caused by heavy precipitation preceding our sampling campaign are responsible for the observed increased levels in major metal concentration fluxes (Fig. 3a). Previous research evaluating changes in dissolved metals has reported a significant increase in Cu and Ni concentrations (filtered <1 μm) following simulated sediment resuspension (Cantwell et al., 2002). On the other hand, the levels of major cations Ca, K, Mg, and Si in surface water were the highest on average during the dry season. We attribute the elevated levels of these major metal concentrations to a combination of erosional processes and increased salinization during the dry season. Close examination of concentration levels during different seasons also indicated specific geochemical behavior of some redox-sensitive metals affected by river flow regimes. For example, high levels of Fe in surface waters were maintained by fluvial-dominated low pH conditions and high river discharge. However, Fe was even higher (up to 0.65 mg/L) during the post-flood sampling event, although pH was above neutral across the sampling transect (Fig. 2C). We suggest that extreme flooding two days before the sampling event have resulted in higher inputs of terrestrial organic matter and humic substances through surface runoff, freshening the system and causing flocculation of metals in coastal water. Fe complexation with humic substances would prevent $Fe(OH)_3$ precipitation from surface waters as Fe preferentially attaches to humic substances in a colloidal state, maintaining high solubility (Namieśnik and Rabajczyk, 2010). Since some colloidal complexes can be smaller than 0.45 μm, they were still present in the 'dissolved' samples and accounted for dissolved Fe in the river discharge during the post-flood sampling event.

PCA results indicate that water depth is the second most important factor for the observed variance of major metal concentrations. For example, crust-associated metals such as Ba, Ca, and Fe have a high positive association with PC2, while the sampling depth is negatively associated with PC2 (Fig. 7A). The spatial distribution of dissolved metals indicated a "hot-spot" pattern of some major metals (e.g., Mg, Ba, Ca, Fe, and K), specifically between SW10 and SW20 where the river near the ash pond perimeter is much shallower (3.5 to 5.5 m) compared to upstream and downstream (7.5 to 9 m) (Appendix B). When considering these two pieces of information, we conclude that shallow depth must facilitate erosion and dissolution of major metals in this section of the river. The observed spatial pattern of higher bedrock-associate metals was persistent regardless of sampling season, further supporting this hypothesis. These effects have previously been observed by others when evaluating the mobilization of metals in dissolved state in a wide range of channel depths and flow velocities (Martin, 2000; Poot et al., 2007).

The third factor explaining the observed metal concentration variations in the study site was contribution of discharged waters from Plant Barry's cooling channel, sampling section between SW18 and SW25. This channel, also called Sister's Creek, was associated with higher conductivity during the dry season and persistent positive temperature anomalies (up to 5 °C) across all sampling events, with a more pronounced signal during the dry and post-flood sampling events. Despite the lack of observed PCA variance and weak correlations between major metal concentrations and temperature across the transect, the individual higher temperatures and dissolution rates of major and toxic metals indicate clear impact of the discharge channel on metal concentrations (Fig. 7). However, we also found that metals such as As, Cd, Co, Cu, Li, Mn, and Sb, were higher between locations near SW16 and SW18 than the sampling transect average during the dry season. At the same

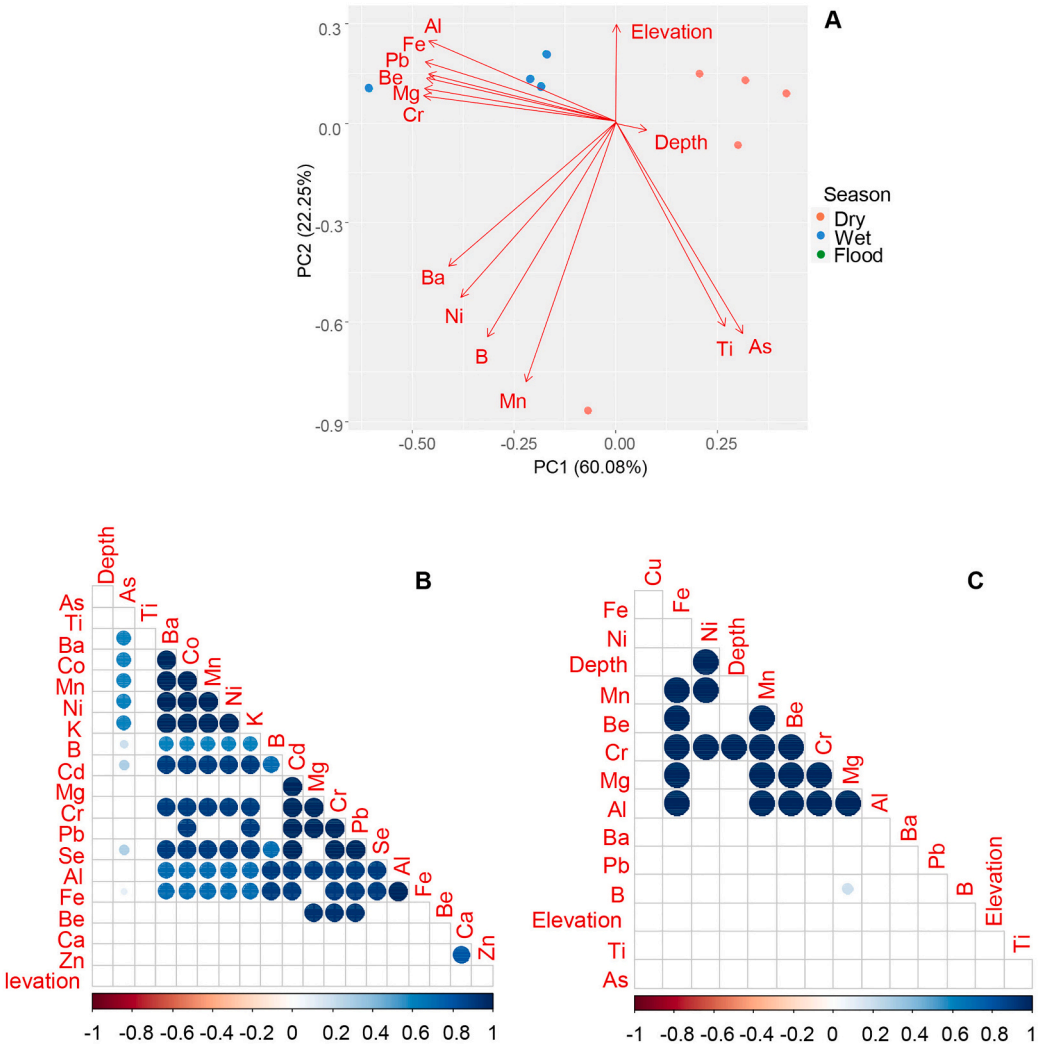

Fig. 8. (A) Principal Component Analyses (PCA) results based on SS metal content assessments in the dry and wet seasons, where red circles represent dry season samples and blue circles represent wet season samples. Also included are Spearman correlation matrices of metal contents of suspended sediments for the (B) dry and (C) wet seasons; blue circles indicate a high positive correlation.

locations (Callaway et al., 2018) detected high levels of toxic metals in groundwater seepage and surface runoff along the perimeter of Pant Barry's ash pond at the previously described shallow water channel depth.

While the seasonal variation of the river discharge and metal concentrations in surface water affected metal fluxes throughout the study area, higher metal levels in surface waters did not always translate into higher fluxes and vice versa. When comparing computed dissolved metal fluxes across sampling events, we found that the major metal fluxes were generally the highest during the post-flood sampling event and the lowest during the dry season, reflecting the river discharge variability and erosional effects from storm events (Fig. 3). Contrary to this general pattern, we found maximum individual Al, Ca, K, and Si fluxes near TIMS-4 (SW 21 and SW22) near the Sister's Creek discharge channel during the dry season when river discharge was the lowest. Specifically, Fe dissolved fluxes downstream near TIMS- 3&4 were several orders of magnitude higher during post-flood conditions than during the dry season, indicating that redox conditions during this sampling event were a primary control. Upstream near TIMS1&2, however, Fe dissolved fluxes were comparable to the rainy season, indicating bedrock erosional and dissolution controls (Fig. 3A). When examining dissolved toxic metal fluxes we found that the As flux was slightly higher during the rainy season than in the dry season (Fig. 3B). In contrast, the estimated average Cd flux throughout the transect was about 2400 kg/day during the dry season, or almost 130 times the wet season SW average of 18.4 kg/day with a maximum flux near TIMS-2, while Cd concentrations during the post-flood sampling event were below detection limits (Fig. 3C).

9.2. *Controls on SS and SS-associated metal fluxes*

Similar to dissolved metals, SS-associated major and toxic metal fluxes were controlled by seasonal variations in river discharge, channel depth, and the contribution from the Sister's Creek discharge channel (Fig. 8). Based on PCA results, during the wet season about two-thirds (60.1 %) of the total variance (PC1) is associated with metal contents such as Al, Be, Cr, Fe, Mg, and Pb, which also increase along the ash pond perimeter (TIMS 2&3). On the other hand, PC2 explains the 22 % total variance of elevated toxic metal content (e.g., As, B, Ba, Mn, Ni, and Ti) in SS at the discharge channel during the dry season (Fig. 8).

We suggest that lower river discharge during the dry season led to more stable environmental conditions and, subsequently (i) higher metal fluxes across all sampler positions and (ii) proportionally higher toxic metal contents from the ash pond discharge channel. High As, Cd, Co, and Ti contents were found across all TIMS locations during the dry season, and the overlaying waters at the respective sites (i.e., SW 12, 17,

and 22) were similarly elevated due to the shallower water depth. We suggest that this is the result of a concentration effect, i.e., having similar metal inventories in smaller volume. Additionally, metal contamination indices indicated the highest As and Cd contamination in SS from the discharge channel at TIMS-4 during the dry season (Fig. 5). In contrast, the wet season with higher river flow disrupted these conditions, resulting in higher major metal contents on average while diluting the effect of the discharge channel. This conclusion is based on both a higher transect average of metal contamination indices (Fe-EF, *Igeo*, CF, and PLI) and strong Spearman correlations of major metal contents Al, Fe, Mg, and toxic metals, including Be, Cu, Cr, and Pb. Note that these metal contents and subsequent metal contamination indices are also higher at sampling locations along the ash pond perimeter (TIMS-2 and TIMS-3), where sediment runoff and resuspension would be more likely to occur. Since all five TIMS were retrieved during the dry season, we could utilize the Gellis Landwhear mixing model and elaborate on the relative spatial overall metal contribution throughout the study site. Mixing model results indicated that sediments collected at TIMS-2 and 3 near the Plant Barry ash pond contributed 81.2 % of the total metal composition downstream. While these results indicate a low contribution of sediments from the downstream discharge channel, they also exemplify the significant contribution of sediments in shallower water depths enriched by the ash pond perimeter during the dry season and lower river discharge.

10. Conclusions

The primary goal of this research was to identify sources of metal contamination present in suspended sediments and surface water in the Mobile River near the Plant Barry ash pond, which could pose a significant environmental hazard to the downstream Gulf Coast. Secondly, we delineated the specific drivers of metals and associated fluxes transported across the 6 km stream stretch by measuring metals in SS and SW over a range of hydrologic conditions and river discharges. We identified a significant contribution of toxic metals (e.g., As, Cd) linked to coal ash near Sister's Creek, the man-made cooling discharge channel of Plant Barry, particularly during the dry season. During this study we detected Cd in SS as high as 4.2 mg/kg, exceeding the 2.2 mg/kg observed in sediments following the Kingston Plant, TN spill in 2016 (Ramsey, 2018; Ramsey et al., 2019). While increased river flow led to substantial upstream erosion and elevated total suspended solids in the river system, the large water flux during the rainy season diluted these signals. However, we found that erosion along the pond's perimeter at shallower depths led to elevated metal fluxes relative to other river sections. Certain dissolved major metal fluxes (e.g., Ca, Mg, Si) were proportional to discharge. In contrast, others, such as Fe, exhibited geochemical changes specifically under high pH and conductivity, altering its levels in surface waters. Contaminated sediments near the pond acted as sources of toxic metals, contributing to increased dissolved metal fluxes (e.g., As, Cd, V) during the dry season.

These findings represent an initial investigation of toxic metal fluxes in aqueous and solid phases and their controlling mechanisms. We recommend that future research encompassing comprehensive environmental sampling, including assessments of organic matter quantity and quality, mineralogical identification, and bulk sediment analysis, to understand better the relationships between metal partitioning and the variable environmental conditions at the Plant Barry ash pond and analogous environments. The outcomes of our study aim to encourage similar research in other anthropogenically impacted aquatic environments and to facilitate a more robust and comprehensive environmental assessment of both short- and long-term contamination stemming from coal ash ponds and related industrial waste sources experiencing seasonal environmental variations.

CRediT authorship contribution statement

Stephen Anderson: Writing – review & editing, Writing – original draft, Visualization, Validation, Methodology, Investigation, Formal analysis, Data curation, Conceptualization. **Natasha T. Dimova:** Writing – review & editing, Writing – original draft, Validation, Supervision, Resources, Project administration, Funding acquisition. **Dini Adyasari:** Writing – review & editing, Visualization, Software, Methodology.

Funding sources

NSF RII Track-2 FEC: Emergent Polymer Sensing Technologies for Gulf Coast Water Quality Monitoring (award # 1632825) granted to N. T.D. S.A. was funded by the Tricampus Materials Science PhD program at the University of Alabama.

Declaration of competing interest

The authors declare the following financial interests/personal relationships which may be considered as potential competing interests: Natasha Dimova reports financial support was provided by NSF EPSCoR Science Information Group. If there are other authors, they declare that they have no known competing financial interests or personal relationships that could have appeared to influence the work reported in this paper.

Acknowledgments

We want to acknowledge the help of the Mobile Bay Keepers and the Dauphin Island Sea Lab for vehicular assistance in collecting field samples during this research. We thank Scott Phipps, National Estuarine Research Reserve Weeks Bay, for logistical support. Finally, we want to thank the two anonymous reviewers who helped us to improve the manuscript.

Appendix A&B. Supplementary data

Supplementary data to this article can be found online at https://doi.org/10.1016/j.scitotenv.2025.179411.

Data availability

Data will be made available on request.

References

Adyasari, D., Montiel, D., Mortazavi, B., Dimova, N., 2021. Storm-driven fresh submarine groundwater discharge and nutrient fluxes from a Barrier Island. Front. Mar. Sci. 8.
Almasoud, F.I., Usman, A.R., Al-Farraj, A.S., 2015. Heavy metals in the soils of the Arabian gulf coast affected by industrial activities: analysis and assessment using enrichment factor and multivariate analysis. Arab. J. Geosci. 8, 1691–1703.
Asgari, S., Badpa, R., Jokar, R., Lonbar, A.G., Karbassi, A., 2023. Enhancement of flocculation processes of metals during estuarine mixing by electrodes. J. Water Process. Eng. 56.
Azziz-Baumgartner, E., Wolkin, A., Sanchez, C., Bayleyegn, T., Young, S., Kieszak, S., Oberst, K., Batts, D., Thomas, C.C., Rubin, C., 2005. Impact of hurricane Ivan on pharmacies in Baldwin County Alabama. J. Am. Pharm. Assoc. 45 (6), 670–675.
Barbieri, M., 2016. The importance of enrichment factor (EF) and geoaccumulation index (Igeo) to evaluate the soil contamination. J. Geol. Geophys. 5 (1), 1–4.
Birch, G.F., Olmos, M.A., 2008. Sediment-bound heavy metals as indicators of human influence and biological risk in coastal water bodies. ICES J. Mar. Sci. 65 (8), 1407–1413.
Braungardt, C.B., Achterberg, E.P., Elbaz-Poulichet, F., Morley, N.H., 2003. Metal geochemistry in a mine-polluted estuarine system in Spain. Appl. Geochem. 18 (11), 1757–1771.
Buat-Menard, P., Chesselet, R., 1979. Variable influence of the atmospheric flux on the trace metal chemistry of oceanic suspended matter. Earth Planet. Sci. Lett. 42 (3), 399–411.
Callaway, C., Kistler, C., Jackson, L., Harrison, P., Johnston, K., Andreen, C., 2018. Coal Ash at Alabama Power's Plant Barry: Mobile Baykeeper Pollution Report Final. Mobile, AL, USA, pp. 5–45.

Cantwell, M.G., Burgess, R.M., Kester, D.R., 2002. Release and phase partitioning of metals from anoxic estuarine sediments during periods of simulated resuspension. Environ. Sci. Technol. 36 (24), 5328–5334.
Davis, R. A. (2017). "sediments of the Gulf of Mexico." habitats and biota of the Gulf of Mexico: before the Deepwater horizon oil spill: volume 1: water quality, sediments, sediment contaminants, oil and gas seeps, coastal habitats, offshore plankton and benthos, and shellfish: 165-215.
Dzwonkowski, B., Park, K., Collini, R., 2015. The coupled estuarine-shelf response of a river-dominated system during the transition from low to high discharge. J. Geophys. Res. Oceans 120 (9), 6145–6163.
Elliott, E.A., Monbureau, E., Walters, G.W., Elliott, M.A., McKee, B.A., Rodriguez, A.B., 2017. A novel method for sampling the suspended sediment load in the tidal environment using bi-directional time-integrated mass-flux sediment (TIMS) samplers. Estuar. Coast. Shelf Sci. 199, 14–24.
Galunin, E., Ferreti, J., Zapelini, I., Vieira, I., Tarley, C. Ricardo Teixeira, Abrão, T., Santos, M.J., 2014. Cadmium mobility in sediments and soils from a coal mining area on Tibagi River watershed: environmental risk assessment. J. Hazard. Mater. 265, 280–287.
Gellis, A.C., Hupp, C.R., Pavich, M.J., Landwehr, J.M., Banks, W.S., Hubbard, B.E., Langland, M.J., Ritchie, J.C., Reuter, J.M., 2009. Sources, Transport, and Storage of Sediment at Selected Sites in the Chesapeake Bay Watershed. U. S. Geological Survey.
Gorny, J., Billon, G., Lesven, L., Dumoulin, D., Madé, B., Noiriel, C., 2015. Arsenic behavior in river sediments under redox gradient: a review. Sci. Total Environ. 505, 423–434.
Haris, H., Looi, L.J., Aris, A.Z., Mokhtar, N.F., Ayob, N.A.A., Yusoff, F.M., Salleh, A.B., Praveena, S.M., 2017. Geo-accumulation index and contamination factors of heavy metals (Zn and Pb) in urban river sediment. Environ. Geochem. Health 39, 1259–1271.
Harkness, J.S., Sulkin, B., Vengosh, A., 2016. Evidence for coal ash ponds leaking in the southeastern United States. Environ. Sci. Technol. 50 (12), 6583–6592.
Hatje, V., Payne, T.E., Hill, D.M., McOrist, G., Birch, G.F., Szymczak, R., 2003. Kinetics of trace element uptake and release by particles in estuarine waters: effects of pH, salinity, and particle loading. Environ. Int. 29 (5), 619–629.
Hsu, L.-C., Huang, C.-Y., Chuang, Y.-H., Chen, H.-W., Chan, Y.-T., Teah, H.Y., Chen, T.-Y., Chang, C.-F., Liu, Y.-T., Tzou, Y.-M., 2016. Accumulation of heavy metals and trace elements in fluvial sediments received effluents from traditional and semiconductor industries. Sci. Rep. 6 (1), 34250.
Hussain, R., Luo, K., Chao, Z., Xiaofeng, Z., 2018. Trace elements concentration and distributions in coal and coal mining wastes and their environmental and health impacts in Shaanxi, China. Environ. Sci. Pollut. Res. 25 (20), 19566–19584.
Idris, A.M., 2008. Combining multivariate analysis and geochemical approaches for assessing heavy metal level in sediments from Sudanese harbors along the Red Sea coast. Microchem. J. 90 (2), 159–163.
Islam, M.S., Ahmed, M.K., Raknuzzaman, M., Habibullah-Al-Mamun, M., Islam, M.K., 2015. Heavy metal pollution in surface water and sediment: a preliminary assessment of an urban river in a developing country. Ecol. Indic. 48, 282–291.
Jegadeesan, G., Al-Abed, S.R., Pinto, P., 2008. Influence of trace metal distribution on its leachability from coal fly ash. Fuel 87 (10), 1887–1893.
Kerr, J.L., Baldwin, D.S., Whitworth, K.L., 2013. Options for managing hypoxic Blackwater events in river systems: a review. J. Environ. Manag. 114, 139–147.
Khaska, M., Le Gal La, C., Salle, P. Verdoux, Boutin, R., 2015. Tracking natural and anthropogenic origins of dissolved arsenic during surface and groundwater interaction in a post-closure mining context: isotopic constraints. J. Contam. Hydrol. 177-178, 122–135.
Lanzerstorfer, C., 2018. Fly ash from coal combustion: dependence of the concentration of various elements on the particle size. Fuel 228, 263–271.
Loska, K., Wiechuła, D., 2003. Application of principal component analysis for the estimation of source of heavy metal contamination in surface sediments from the Rybnik reservoir. Chemosphere 51 (8), 723–733.
Martin, C.W., 2000. Heavy metal trends in floodplain sediments and valley fill, river Lahn, Germany. CATENA 39 (1), 53–68.
Martínez, L.L.G., Poleto, C., 2014. Assessment of diffuse pollution associated with metals in urban sediments using the geoaccumulation index (I geo). J. Soils Sediments 14, 1251–1257.
Mehra, A., Farago, M., Banerjee, D., 1998. Impact of fly ash from coal-fired power stations in Delhi, with particular reference to metal contamination. Environ. Monit. Assess. 50 (1), 15–35.
Melaku, S., Dams, R., Moens, L., 2005. Determination of trace elements in agricultural soil samples by inductively coupled plasma-mass spectrometry: microwave acid digestion versus aqua regia extraction. Anal. Chim. Acta 543 (1-2), 117–123.
Miller, J. and K. G. Robinson (1995). A regional perspective of the physiographic provinces of the southeastern United States.
Miranda, L.S., Ayoko, G.A., Egodawatta, P., Goonetilleke, A., 2022. Adsorption-desorption behavior of heavy metals in aquatic environments: influence of sediment, water and metal ionic properties. J. Hazard. Mater. 421, 126743.
Montiel, D., Dimova, N., Andreo, B., Prieto, J., García-Orellana, J., Rodellas, V., 2018. Assessing submarine groundwater discharge (SGD) and nitrate fluxes in highly heterogeneous coastal karst aquifers: challenges and solutions. J. Hydrol. 557, 222–242.
Namieśnik, J., Rabajczyk, A., 2010. The speciation and physico-chemical forms of metals in surface waters and sediments. Chem. Speciat. Bioavailab. 22 (1), 1–24.
Oksanen, J., Blanchet, F.G., Kindt, R., Legendre, P., Minchin, P.R., O'hara, R., Simpson, G.L., Solymos, P., Stevens, M.H.H., Wagner, H., 2013. "Package 'vegan'." Community ecology package. version 2 (9), 1–295.
Paul, V., Sankar, M., Vattikuti, S., Dash, P., Arslan, Z., 2021. Pollution assessment and land use land cover influence on trace metal distribution in sediments from five aquatic systems in southern USA. Chemosphere 263, 128243.
Peng, G., 2008. Understanding watershed suspended sediment transport. Prog. Phys. Geog.: Earth Environ. 32 (3), 243–263.
Perez-Santana, S., Alfonso, M.P., Tagle, M.V., Icart, M.P., Brunori, C., Morabito, R., 2007. Total and partial digestion of sediments for the evaluation of trace element environmental pollution. Chemosphere 66 (8), 1545–1553.
Poot, A., Gillissen, F., Koelmans, A.A., 2007. Effects of flow regime and flooding on heavy metal availability in sediment and soil of a dynamic river system. Environ. Pollut. 148 (3), 779–787.
Ramsey, A.B., 2018. Assessment of Sustained Impacts from the Kingston Fossil Plant Coal Ash Spill on Surface Water and River Sediments in Eastern Tennessee.
Ramsey, A.B., Faiia, A.M., Szynkiewicz, A., 2019. Eight years after the coal ash spill–fate of trace metals in the contaminated river sediments near Kingston, eastern Tennessee. Appl. Geochem. 104, 158–167.
Roseburrough, R.R., Wang, X., 2019. Chromium distribution in water and sediments in the Mobile River and bay, Alabama. Gulf Carib. Res. 30.
Ruhl, L., Vengosh, A., Dwyer, G.S., Hsu-Kim, H., Deonarine, A., 2010. Environmental impacts of the coal ash spill in Kingston, Tennessee: an 18-month survey. Environ. Sci. Technol. 44 (24), 9272–9278.
Smedley, P.L., Kinniburgh, D.G., 2002. A review of the source, behaviour and distribution of arsenic in natural waters. Appl. Geochem. 17 (5), 517–568.
Stewart, J., 2020. Watershed-Estuary Dynamics in the Mobile River Watershed-Mobile Bay Estuary (Mr-Mb) Continuum Examined by Combined Geochemical and Satellite Approaches. The University of Alabama.
Totten, R.L., Parker, L.E., Wallace, D.J., Lambert, W.J., Elliott, E.A., Andrus, C.F.T., Lehrmann, A.A., 2020. A 7000-year record of floods and ecological feedbacks in Weeks Bay, Alabama, USA. Sci. Total Environ. 743, 140052.
Vengosh, A., Cowan, E.A., Coyte, R.M., Kondash, A.J., Wang, Z., Brandt, J.E., Dwyer, G. S., 2019. Evidence for unmonitored coal ash spills in Sutton Lake, North Carolina: implications for contamination of lake ecosystems. Sci. Total Environ. 686, 1090–1103.
Villaescusa-Celaya, J.A., Gutiérrez-Galindo, E.A., Flores-Muñoz, G., 2000. Heavy metals in the fine fraction of coastal sediments from Baja California (Mexico) and California (USA). Environ. Pollut. 108 (3), 453–462.
Wang, N., Ye, Z., Huang, L., Zhang, C., Guo, Y., Zhang, W., 2023. Arsenic occurrence and cycling in the aquatic environment: a comparison between freshwater and seawater. Water 15 (1), 147.
Wang, Z., Cowan, E.A., Seramur, K.C., Dwyer, G.S., Wilson, J.C., Karcher, R., Brachfeld, S., Vengosh, A., 2022. Legacy of coal combustion: widespread contamination of Lake sediments and implications for chronic risks to aquatic ecosystems. Environ. Sci. Technol. 56 (20), 14723–14733.
Warner, K.A., 2005. Effect of watershed parameters on mercury distribution in different environmental compartments in the Mobile Alabama River basin, USA. Sci. Total Environ. 347 (1−30), 187–207.
Warner, K.A., Bonzongo, J.-C.J., Roden, E.E., Ward, G.M., Green, A.C., Chaubey, I., Lyons, W.B., Arrington, D.A., 2005. Effect of watershed parameters on mercury distribution in different environmental compartments in the Mobile Alabama River basin, USA. Sci. Total Environ. 347 (1–3), 187–207.
Wen, L.-S., Santschi, P.H., Gill, G.A., Paternostro, C.L., Lehman, R.D., 1997. Colloidal and particulate silver in river and estuarine waters of Texas. Environ. Sci. Technol. 31 (3), 723–731.
Wen, L.-S., Santschi, P., Gill, G., Paternostro, C., 1999. Estuarine trace metal distributions in Galveston Bay: importance of colloidal forms in the speciation of the dissolved phase. Mar. Chem. 63 (3), 185–212.
Xu, J., Yu, D., Fan, B., Zeng, X., Lv, W., Chen, J., 2014. Characterization of ash particles from co-combustion with a Zhundong coal for understanding ash deposition behavior. Energy Fuel 28 (1), 678–684.
Yaqin, J., Yinchang, F., Jianhui, W., Tan, Z., Zhipeng, B., Chiqing, D., 2008. Using geoaccumulation index to study source profiles of soil dust in China. J. Environ. Sci. 20 (5), 571–578.
Zhang, J., Liu, C., 2002. Riverine composition and estuarine geochemistry of particulate metals in China—weathering features, anthropogenic impact and chemical fluxes. Estuar. Coast. Shelf Sci. 54 (6), 1051–1070.
Zhu, W., Zhang, X., Zhu, Z., Fu, W., Liu, N., Zhang, Z., 2024. A rapid detection method for coal ash content in tailings suspension based on absorption spectra and deep feature extraction. Mathematics 12 (11), 1685.